Lagrangian conditional statistics, acceleration and local relative motion in numerically simulated isotropic turbulence

P. K. YEUNG[1], S. B. POPE[2], E. A. KURTH[1] AND A. G. LAMORGESE†[2]

[1]School of Aerospace Engineering, Georgia Institute of Technology, Atlanta, GA 30332, USA
[2]Sibley School of Mechanical and Aerospace Engineering,
Cornell University, Ithaca, NY 14853, USA

Lagrangian statistics of fluid-particle velocity and acceleration conditioned on fluctuations of dissipation, enstrophy and pseudo-dissipation representing different characteristics of local relative motion are extracted from a direct numerical simulation database of stationary (forced) homogeneous isotropic turbulence. The grid resolution in the simulations is up to 2048^3, and the Taylor-scale Reynolds number ranges from about 40 to 650, where characteristics of small-scale intermittency in the Eulerian flow field are well developed. A key joint statistic of the conditioning variables is the dissipation–enstrophy cross-correlation, which is asymmetric, but becomes less so at high Reynolds number. Conditional velocity autocorrelations are consistent with rapid changes in the velocity of fluid particles moving in regions of large velocity gradients. Examination of statistics conditioned upon enstrophy, especially in a local coordinate frame moving with the vorticity vector, and of the centripetal acceleration suggests the presence of vortex-trapping effects which persist for several Kolmogorov time scales. Further results on acceleration statistics and joint velocity–acceleration autocorrelations are also presented to help characterize in detail the properties of a joint stochastic process of velocity, acceleration and the pseudo-dissipation. Together with recent work on Eulerian conditional acceleration and Reynolds-number dependence of basic Lagrangian quantities, the present results are directly useful for the development of a new stochastic model formulated to account for intermittency and Reynolds-number effects as described in detail in a companion paper.

1. Introduction

The Lagrangian approach of following the motions of infinitesimal fluid elements has long been recognized (Taylor 1921; Monin & Yaglom 1975) as central in descriptions of turbulent transport and dispersion. It is clear that the spatial structure of the turbulence plays an important role: namely, the large-scale motions determine integral time scales and particle displacement, whereas local relative motion in the form of turbulent straining and rotation determines changes of fluid-particle velocity with time and between different particles which diffuse relative to each other. In

† Present address: CTR/Stanford University, Bldg 500, Stanford, CA 94305, USA.

particular, fluid particles moving in a region of large velocity gradients can be expected to experience rapid changes in velocity, i.e. a large acceleration, whose magnitude and direction may depend on whether high strain rate or high rotation rate is involved. One effective strategy for investigating the effects of local flow structure is thus to sample Lagrangian trajectories conditionally, according to certain measures of the intensity of local strain, rotation, or velocity gradients in general. This approach has been used with success (Yeung *et al.* 2006*a*) in an Eulerian frame where we study acceleration as the material derivative of velocity according to the Navier–Stokes equations. Consideration of intermittency via a model for the Lagrangian acceleration (Sawford 1991; Pope 2002; Reynolds 2003*a*) is important for incorporating Reynolds-number dependence in stochastic modelling. Recent interest in various aspects of the acceleration (e.g. LaPorta *et al.* 2001; Sawford *et al.* 2003; Biferale *et al.* 2004) also provides further motivation for examining the effects of small-scale intermittency on statistics of Lagrangian fluid-particle motion.

Our main purpose in this paper is to present a detailed numerical investigation of the effects of local flow structure over a substantial Reynolds-number range on the Lagrangian statistics of velocity and acceleration. The central theme is to advance fundamental understanding while providing data for model development. The nature of local relative motion in the flow may be characterized by fluctuations of the energy dissipation rate ($\epsilon \equiv 2\nu s_{ij}s_{ij}$), enstrophy ($\zeta \equiv \nu\omega_i\omega_i$), or pseudo-dissipation ($\varphi \equiv \nu(\partial u_i/\partial x_j)^2$), where in these definitions ν, s_{ij}, ω_i and $\partial u_i/\partial x_j$ denote kinematic viscosity, strain rate, vorticity and the velocity gradient tensor, respectively. For example, the autocorrelation between fluid particle velocity at times t and $t+\tau$ (where τ is a time lag) conditioned upon the value of energy dissipation at the particle position at time t gives information on the effects of local strain rate on the Lagrangian statistics of the flow. Likewise, if there is a tendency for fluid particles to be trapped in regions of high vorticity (Biferale *et al.* 2005; Bec *et al.* 2006; Xu *et al.* 2006) this should be quantifiable via the sensitivity of Lagrangian statistics to enstrophy as a conditioning variable.

Because local relative motion is inherently dominated by the small scales, classical concepts of small-scale universality suggest that forced stationary isotropic turbulence is, although idealized, an appropriate flow configuration for the present study. A further advantage is that this flow is most readily amenable to the use of advanced computing power to obtain data at the highest Reynolds number possible. It should be noted that conditional statistics of the types mentioned above require accurate data at a very high level of detail – essentially all coordinate components of velocity and velocity gradient fluctuations along a large number of irregular particle trajectories. Despite advances in Lagrangian measurements (Voth, Satyanarayan & Bodenschatz 1998; Mordant *et al.* 2001; Berg *et al.* 2006; Guala *et al.* 2006; Ouellette, Xu & Bodenschatz 2006), the data we require are, at present, best obtained from direct numerical simulation (DNS) with a high-order interpolation scheme (Yeung & Pope 1988) which can provide the time history of many flow variables along the particle trajectories (Yeung 2002). Lagrangian statistics of dissipation, enstrophy and pseudo-dissipation from DNS have been reported in Yeung & Pope (1989), and Yeung *et al.* (2006*b*). However, conditional Lagrangian statistics with these quantities used as the conditioning variables appear to be new to the literature, with the possible exception of Luthi, Tsinober & Kinzelbach (2005) who used wide sampling bins in experiments at low Reynolds number. Conditional sampling based on these highly intermittent variables is more challenging than that based on the velocity previously considered by other authors (Sawford *et al.* 2003; Mordant, Crawford & Bodenschatz 2004; Crawford, Mordant & Bodenschatz 2005).

N	64	128	256	512	1024	2048
R_λ	43	86	140	235	393	648
ν	0.025	0.0071	0.0028	0.0011	0.000437	0.0001732
$\langle \epsilon \rangle$	1.31	1.17	1.17	1.20	1.26	1.10
L_1/η	24	52	98	201	450	732
T_L/τ_η	5.4	8.6	13.1	19.8	31.1	43.8
$k_{max}\eta$	1.77	1.41	1.41	1.40	1.37	1.44
T/T_L	32.3	36.3	15.5	10.7	10.0	6.0
$\Delta t/\tau_\eta$	0.0432	0.0328	0.0191	0.0166	0.0101	0.00066
h/τ_η	0.217	0.193	0.184	0.198	0.215	0.243

TABLE 1. Major parameters of the numerical simulation database.

The numerical simulation database analysed in this paper is the same as that reported in Yeung *et al.* (2006*b*), at grid resolution up to 2048^3 and Taylor-scale Reynolds number (R_λ) up to about 650. Table 1 gives some numerical parameters, including the range of scales in length and time in terms of longitudinal integral length scale (L_1), Lagrangian velocity integral time scale (T_L), Kolmogorov scales of length and time (η, τ_η), resolution of the small scales in terms of highest wavenumber resolved ($k_{max} = \sqrt{2}N/3$ on an N^3 grid), time duration of the simulation (T) compared with T_L, and average DNS time step (Δt) as well as Lagrangian sampling time interval (h) compared with τ_η. The largest (2048^3) simulation was performed at Pittsburgh Supercomputing Center. As discussed in Yeung *et al.* (2006*b*), all of the simulations listed have the same forcing parameters, but different viscosities. In all cases, we maintain a constant Courant number (close to 0.6) which makes Δt small compared to τ_η at increasing N and R_λ, while fluid particle properties are saved at time intervals $h = O(1/4\tau_\eta)$ or less for analysis. The simulation at highest grid resolution (2048^3) is shorter in terms of T_L because of CPU expense, but still adequate, especially since our present focus is on small-scale quantities that have relatively short time scales.

An important motivation in DNS is to contribute to model development as well as physical understanding. In particular, the numerical study reported in this paper is, in part, guided by a need for specific test results for a new stochastic model described in detail in an accompanying paper (Lamorgese *et al.* 2007). The proposed model represents conceptual advancements over previous work (Sawford 1991; Reynolds 2003*b*) in its treatment of intermittency, which is implemented by incorporating a non-Gaussian model for the acceleration conditioned upon fluctuations of the pseudo-dissipation rate (φ). Use of φ instead of the energy dissipation rate (ϵ) as a descriptor of intermittency is appropriate here because it naturally includes the effects of both local strain and rotation, and because it has been shown in DNS (Yeung *et al.* 2006*a*) to be closer to log-normal. In addition, the acceleration conditioned on φ (rather than on ϵ or ζ) has the smallest variance and is represented well by a simple ('cubic-Gaussian') probability density function (PDF). The model of Lamorgese *et al.* (2007) consists of coupled stochastic differential equations (SDEs) for pseudo-dissipation, acceleration and velocity. Specifically, and consistent with the above observations: $\ln \varphi$ is modelled by an Ornstein–Uhlenbeck process; the SDE for acceleration yields a conditionally cubic-Gaussian distribution; and the (degenerate) SDE for velocity amounts to the exact relation of velocity being the integral of acceleration. Quantities crucial to such a model description therefore include one- and two-time statistics of the velocity and acceleration, taken separately or jointly, conditioned upon the pseudo-dissipation. For example, conditional autocorrelations of both velocity and acceleration presented in

this paper have been used for model development and testing by Lamorgese *et al.* (2007). Likewise, conditional and unconditional structure functions of the velocity are reported in Lamorgese *et al.* (2007) and used to show that the new model achieves better agreement with DNS over previous work by Reynolds (2003*b*) which assumed a conditionally Gaussian acceleration given the energy dissipation rate.

In §2, we give a brief summary of the numerical methods used to perform the simulation and analyse the data, including specific issues that arise in the processing of auto- and cross-correlation functions conditioned on either ϵ, ζ or φ. Current results on the autocorrelations of these three conditioning variables have been given in Yeung *et al.* (2006*b*), together with basic information on the velocity structure function and frequency spectrum interpreted in terms of classical Kolmogorov scaling. Some additional background results on the joint statistics of these variables are first given in §3. Results on conditional statistics are given in §§4–6, for velocity and acceleration considered separately, and then jointly as a pair of random variables. In §4, we observe that, when the Reynolds number is low, the velocity autocorrelation conditioned on high enstrophy has some special features which can be interpreted as evidence of fluid particles trapped in regions of high vorticity (Biferale *et al.* 2005). A decomposition of the velocity vector in local coordinate axes parallel and perpendicular to the vorticity vector is used to help explain this effect, which becomes weaker at high Reynolds number. In §5, we present acceleration–dissipation cross-correlations followed by acceleration autocorrelations conditioned on the dissipation variables. In §6, we present both unconditional and conditional versions of the cross-correlation between velocity and acceleration. We conclude this paper in §7 with a summary of the DNS results and and their role in stochastic modelling.

2. Numerical approach

The basic elements of our numerical simulation approach are as described in several previous publications (e.g. Yeung 2001; Yeung *et al.* 2006*b*): namely, the well-known Fourier pseudo-spectral approach of Rogallo (1981) coupled with the particle-tracking algorithm of Yeung & Pope (1988). Stochastic forcing at the large scales (Eswaran & Pope 1988) is used to maintain a statistically stationary state and allow higher Reynolds numbers to be sustained on a given grid. Cubic spline interpolation, which is fourth-order accurate and twice-differentiable, is used to calculate velocity and velocity gradients (hence the quantities ϵ, ζ, φ) along the trajectories of a large number of fluid particles with randomly distributed initial positions. The smoothness properties of cubic splines also facilitate the calculation of acceleration by a simple finite difference in time from velocity time series saved at intervals (h) of order $1/4$ of a Kolmogorov time-scale (τ_η) or less apart. Theoretical arguments based on intermittency (Yakhot & Sreenivasan 2005) have suggested that accurate results for acceleration statistics (especially the higher-order moments) may require the small scales to be resolved to a degree beyond prevailing practices in DNS. However, in Yeung *et al.* (2006*a*) we show that these effects are weaker for statistics of acceleration conditioned upon fluctuations of ϵ, ζ or φ since the conditional variables are inherently less intermittent.

Knowledge of conditional averages in turbulence is valuable because they provide a quantifiable measure of the statistical coupling between fluctuations in one flow variable and another, and because they are needed as unclosed terms in PDF modelling where a Lagrangian viewpoint is frequently adopted (Pope 1985). However, most available DNS data on conditional statistics in the literature (e.g. Kronenburg & Bilger 1997; Vedula, Yeung & Fox 2001) are Eulerian, with all variables involved

taken at the same grid points. In the Lagrangian frame, we have a choice of whether to take the conditioning variable at, say, the beginning or the end of a time interval from t to $t + \tau$. However, conditioning on the 'present' (time t) is more natural for stochastic modelling aimed at predicting the future (time $t + \tau$). With superscript $^+$ denoting Lagrangian quantities and $u^+(t)$ being a component of the fluid particle velocity, we can define the conditional velocity autocorrelation given a random variable $Z^+(t)$ (which may be ϵ, ζ or φ) as

$$\rho_u(\tau|Z) \equiv \frac{\langle u^+(t)u^+(t+\tau)|Z^+(t) = Z\rangle}{\langle (u^+(t))^2|Z^+(t) = Z\rangle}, \tag{2.1}$$

where Z is the corresponding sample-space variable for $Z^+(t)$. Because of stationarity, both the numerator and denominator above can be averaged over time t within the entire period of the simulation. Computation of the numerator requires both conditional sampling for each particle over the distribution of $Z^+(t)$ divided into suitable histogram bins, and the averaging over many intervals of size τ within a finite overall simulation period (T). From (2.1), it can be seen that $\rho_u(\tau|Z)$ equals unity at $\tau = 0$ (as for its unconditional counterpart), but (because of the normalization chosen) is not strictly bounded between -1 and 1. A negative τ corresponds to conditioning on $Z^+(t + \tau)$ at the end of the interval $[t, t + \tau]$. In most instances, we choose histogram bins for $Z^+(t)$ (which may be ϵ, ζ or φ) based on their logarithms, which are approximately Gaussian (Yeung *et al.* 2006a).

Conditioning on enstrophy (in the manner of (2.1)) provides information on the Lagrangian history of fluid particles moving in regions of high vorticity, which is relevant to the issue of fluid particles trapped in vortical regions in turbulent flow (Biferale *et al.* 2005). Clearly, the statistics of velocity components along and perpendicular to the axis of a strong vortex are expected to differ. To characterize these effects, it is useful to project the velocity vector onto a system of local coordinate axes consisting of a unit vector along the direction of local vorticity, and two unit vectors which rotate in the orthogonal plane according to the local rotation-rate tensor. Specifically, let $\boldsymbol{\xi}(t)$, $\boldsymbol{p}(t)$, $\boldsymbol{q}(t)$ be mutually orthogonal unit vectors, with $\boldsymbol{\xi}(t) = \boldsymbol{\omega}(t)/|\boldsymbol{\omega}(t)|$. We allow $\boldsymbol{p}(t)$ and $\boldsymbol{q}(t)$ to rotate according to the fluctuating rate-of-rotation tensor $\boldsymbol{R}(t)$, but require them to remain orthogonal to $\boldsymbol{\xi}(t)$ (and to each other). These conditions are met if we let $\boldsymbol{p}(t)$ and $\boldsymbol{q}(t)$ evolve by the pair of (identical) equations

$$\frac{\mathrm{d}\boldsymbol{p}}{\mathrm{d}t} = \boldsymbol{R}\boldsymbol{p} - \boldsymbol{\xi}(\boldsymbol{p} \cdot \mathrm{d}\boldsymbol{\xi}/\mathrm{d}t), \quad \frac{\mathrm{d}\boldsymbol{q}}{\mathrm{d}t} = \boldsymbol{R}\boldsymbol{q} - \boldsymbol{\xi}(\boldsymbol{q} \cdot \mathrm{d}\boldsymbol{\xi}/\mathrm{d}t). \tag{2.2}$$

From these equations it can be readily shown that if $\boldsymbol{\xi}(t)$, $\boldsymbol{p}(t)$, $\boldsymbol{q}(t)$ are initially orthogonal, then the time derivatives of dot products between any two of them vanish; thus they should remain mutually orthogonal at all times. Initial conditions are generated by using a Craya decomposition: e.g. let $\boldsymbol{e}^{(1)}$ be the unit vector along the x_1-axis in a fixed coordinate system, then defining

$$\boldsymbol{p}(0) = \left(\boldsymbol{\xi}(0) \times \boldsymbol{e}^{(1)}\right)/\left|\boldsymbol{\xi}(0) \times \boldsymbol{e}^{(1)}\right|, \quad \boldsymbol{q}(0) = (\boldsymbol{\xi}(0) \times \boldsymbol{p}(0))/|\boldsymbol{\xi}(0) \times \boldsymbol{p}(0)|. \tag{2.3}$$

For numerical integration from time level t_n to $t_{n+1} = t_n + h$ we use a second-order predictor–corrector scheme similar to that for time advancement in the DNS code, with the time derivative $\mathrm{d}\boldsymbol{\xi}/\mathrm{d}t$ computed from the Lagrangian time series of vorticity using second-order central differences. In practice, the interval h can only be as small as the time interval at which we collect Lagrangian time series in the simulations: usually this is about $1/4$ of τ_η, which may not be small enough to capture rapid

variations of the change of vorticity vector orientation. To correct for discretization errors due to the finiteness of h we enforce orthogonality at each time level using the projection tensor based on $\boldsymbol{\xi}(t_{n+1})$: i.e. the numerical solution $\hat{\boldsymbol{p}}$ to (2.2) at time t_{n+1} is converted to $p_i(t_{n+1}) = P_{ij}(\boldsymbol{\xi}(t_{n+1}))p_j$, where $P_{ij}(\boldsymbol{\xi}) = \delta_{ij} - \xi_i\xi_j$. The effectiveness of this correction procedure has been checked by forming the PDF of $\boldsymbol{\xi} \cdot \boldsymbol{p}$ before and after the correction at each time step, and by comparing results with a 64^3 simulation in which we used a value of h as small as $1/16$ of τ_η. We refer to the velocity component along the vorticity vector as $u_\parallel$ whereas the two components along $\boldsymbol{p}(t)$ and $\boldsymbol{q}(t)$ are statistically equivalent and referred to as $u_\perp$.

Lagrangian properties of each of the variables ϵ, ζ and φ taken separately provide important background information for interpreting velocity and acceleration statistics conditioned on these quantities. Results on ϵ, ζ and φ taken separately have been presented in Yeung *et al.* (2006b). These variables are found to have approximately exponential autocorrelations with integral time scales which decrease with respect to T_L but increase relative to τ_η as the Reynolds number increases. In contrast to results by Yeung & Pope (1989), at high Reynolds number, dissipation and enstrophy are found to have similar time scales whereas the logarithms of ϵ, ζ and φ all have longer time scales that appear to follow T_L. The results also suggest that modelling as a diffusion process with Gaussian statistics is more appropriate for $\ln\varphi$ than for $\ln\epsilon$.

In this paper, we include cross-correlations between pairs of random variables. As a generic definition for two Lagrangian variables X and Y of mean values μ_X, μ_Y and variances $\text{Var}(X)$, $\text{Var}(Y)$, we write

$$\rho_{XY}(\tau) \equiv \frac{\langle (X^+(t) - \mu_X)((Y^+(t+\tau) - \mu_Y) \rangle}{\{\text{Var}(X)\text{Var}(Y)\}^{1/2}}, \tag{2.4}$$

where the denominator is averaged over the entire time record of each simulation. The variable $X^+(t)$ is considered to be leading in time if $\tau > 0$, but lagging if $\tau < 0$. Although stationarity requires $\rho_{XY}(-\tau) = \rho_{YX}(\tau)$, this relation does not carry over to the conditional cross-correlation given another variable Z at time t, i.e. in general $\rho_{XY}(-\tau|Z)$ (defined by replacing τ by $-\tau$ in Eq. 2.4) is not the same as $\rho_{YX}(\tau|Z)$. At $\tau = 0$, the single-time correlation coefficient is recovered, which is also written simply as $\rho(X, Y)$.

3. Dissipation–enstrophy cross-correlations

Although in most studies in the literature (e.g. Yeung & Pope 1989; Chen, Sreenivasan & Nelkin 1997; Zhou & Antonia 2000) enstrophy is found to be more intermittent than the dissipation, there is considerable interest in whether their statistics may scale similarly at high Reynolds number (Sreenivasan & Antonia 1997; Nelkin 1999). From a Lagrangian perspective, diagnostics useful for this issue include the autocorrelations of these quantities (Yeung *et al.* 2006b), and their cross-correlations (Yeung & Pope 1989), shown in figure 1 for six simulations with $R_\lambda \approx 40 - 650$ (as in table 1) and time lag normalized by T_L. Because both of these variables evolve on time scales shorter than T_L, as the Reynolds number increases all six curves shown become narrower under this scaling. A more significant observation is the asymmetry of stronger correlation for $\tau > 0$. Physically, this suggests fluid particles are more likely to experience high dissipation followed by high enstrophy versus high enstrophy followed by high dissipation. Alternatively, this also suggests events of high enstrophy are more intermittent and last for shorter periods of time than those of high dissipation. The degree of asymmetry in figure 1 can be quantified
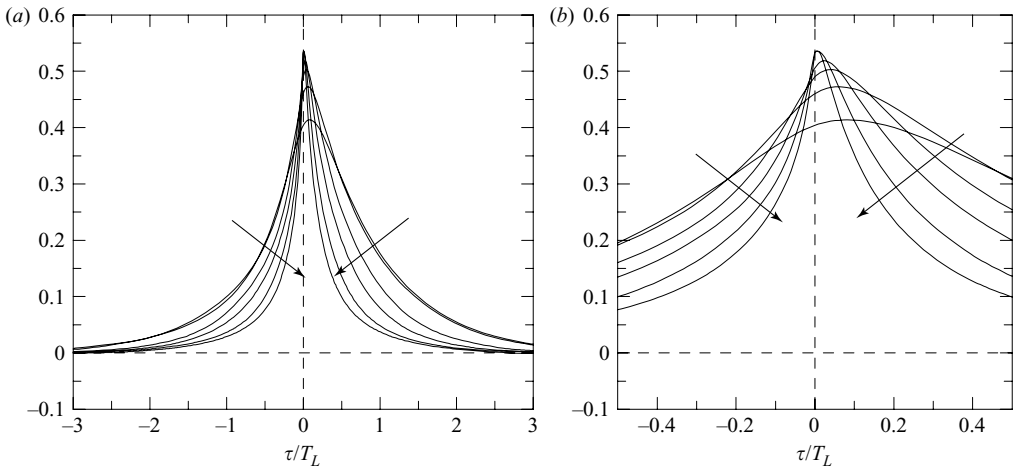
FIGURE 1. (*a*) Dissipation–enstrophy cross-correlation functions $[\rho_{\epsilon\zeta}(\tau)]$ at the six Reynolds numbers ($R_\lambda \approx 40$, 90, 140, 240, 390, 650) as recorded in table 1. (*b*) A blow up of data at smaller $|\tau|$. Arrows indicate trend of increasing Reynolds number (note there is some non-monotonic behaviour at small $|\tau|$).

N	64	128	256	512	1024	2048
R_λ	43	86	140	235	393	648
$\mathscr{T}_+/T_L$	0.429	0.488	0.435	0.417	0.376	0.367
$\mathscr{T}_-/T_L$	0.271	0.316	0.285	0.283	0.272	0.281
$\mathscr{T}_+/\mathscr{T}_-$	1.582	1.541	1.528	1.473	1.380	1.308
$\rho(\epsilon, \zeta)$	0.311	0.402	0.449	0.493	0.537	0.571

TABLE 2. Ratio of areas under positive and negative time lags in the dissipation–enstrophy cross-correlation, and single-time correlation (taken at $\tau = 0$).

by comparing the areas under the curves for the ranges of $\tau < 0$ versus $\tau > 0$: i.e. the time scales $\mathscr{T}_+ = \int_0^\infty \rho_{\epsilon\zeta}(\tau)\mathrm{d}\tau$ and $\mathscr{T}_- = \int_{-\infty}^0 \rho_{\epsilon\zeta}(\tau)\,\mathrm{d}\tau$ (table 2). It is clear that at higher Reynolds number, the cross-correlation function shows an increase in the degree of symmetry, which implies that events of high dissipation followed by high enstrophy and high enstrophy followed by high dissipation along the particle trajectory approach become more equally probable. Closer examination (figure 1*b*) also indicates an increase in the cross-correlation coefficient (at $\tau = 0$). These observations are consistent with suggestions from Eulerian work (Yeung, Donzis & Sreenivasan 2005) of a tendency for the statistics of dissipation and enstrophy to become more similar at higher Reynolds numbers.

Given the wide range of Reynolds numbers in our database, it is helpful to make more detailed comparisons for data at the lowest and highest as well as an intermediate Reynolds number. For the latter, we choose the 256^3 data at $R_\lambda \sim 140$, which is close to the value of R_λ at which recognizable inertial-range features begin to appear in the Eulerian energy spectrum (Yeung & Zhou 1997). Accordingly, in figure 2 we show data from our 64^3, 256^3 and 2048^3 simulations on cross-correlations for the three pairs of variables formed from ϵ, ζ and φ. As the Reynolds number increases, these curves drop significantly faster with increasing τ/T_L whereas normalization by τ_η produces a modest but imperfect degree of collapse. This is consistent with observations
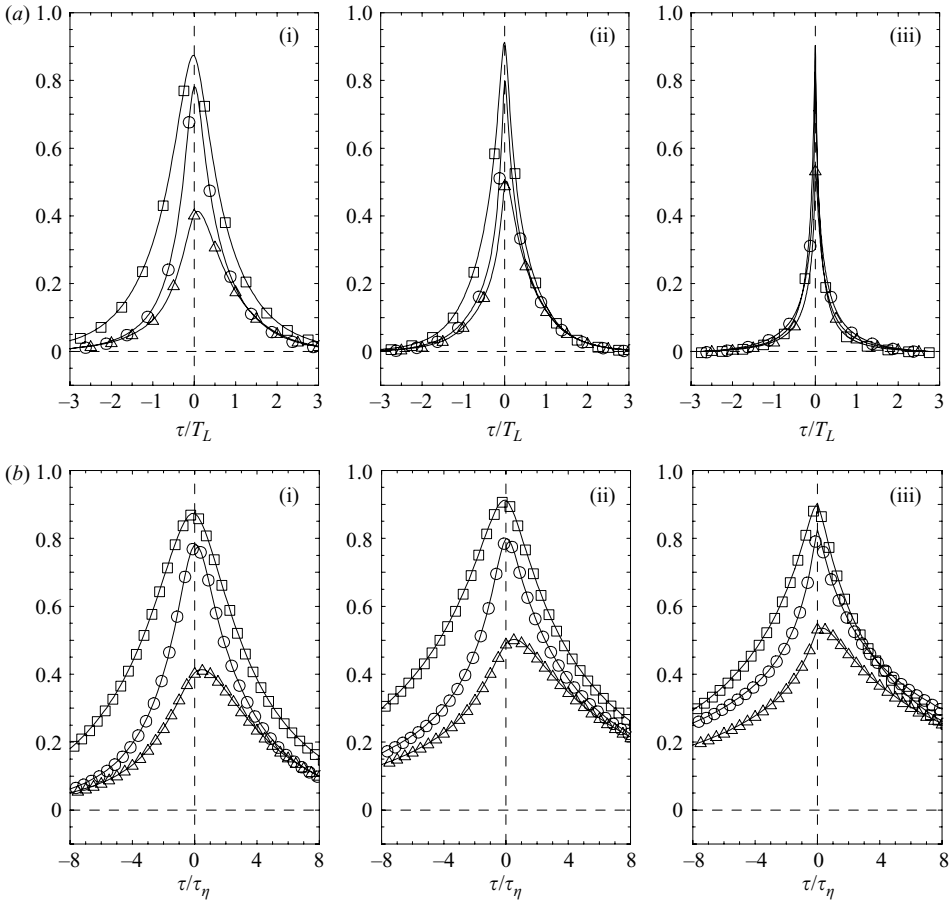
FIGURE 2. Cross-correlations $\rho_{\epsilon\zeta}(\tau)$ (triangles), $\rho_{\epsilon\varphi}(\tau)$ (circles) and $\rho_{\zeta\varphi}(\tau)$ (squares) at (i) $R_\lambda \approx 40$, (ii) 140 and (iii) 650 (grid resolutions 64^3, 256^3, 2048^3 respectively) in our simulations. Normalizing time scales are (a) T_L and (b) τ_η.

from single-variable autocorrelations which are best considered as possessing two characteristic time scales (Yeung *et al.* 2006b).

It can be seen that the cross-correlation between ζ and φ is the strongest among the three quantities shown in figure 2, but differences become small at high Reynolds number as the cross-correlations start to fall more rapidly with τ/T_L (but less rapidly with respect to τ_η). These features can be explained in part by using the identity $\varphi = (\epsilon + \zeta)/2$ to obtain the relations

$$\rho_{\epsilon\varphi}(\tau) = \frac{1}{2}\left[\frac{\sigma_\epsilon}{\sigma_\varphi}\rho_\epsilon(\tau) + \frac{\sigma_\zeta}{\sigma_\varphi}\rho_{\epsilon\zeta}(\tau)\right], \qquad (3.1)$$

$$\rho_{\zeta\varphi}(\tau) = \frac{1}{2}\left[\frac{\sigma_\zeta}{\sigma_\varphi}\rho_\zeta(\tau) + \frac{\sigma_\epsilon}{\sigma_\varphi}\rho_{\epsilon\zeta}(-\tau)\right], \qquad (3.2)$$

where $\rho_\epsilon(\tau)$ and $\rho_\zeta(\tau)$ are the dissipation and enstrophy autocorrelations. Because (except perhaps at very high Reynolds numbers) enstrophy has a larger variance and a more persistent autocorrelation, the first term in (3.2) makes $\rho_{\zeta\varphi}(\tau)$ larger than $\rho_{\epsilon\varphi}(\tau)$, as observed. For $\tau > 0$, this effect is partly compensated by the second term in
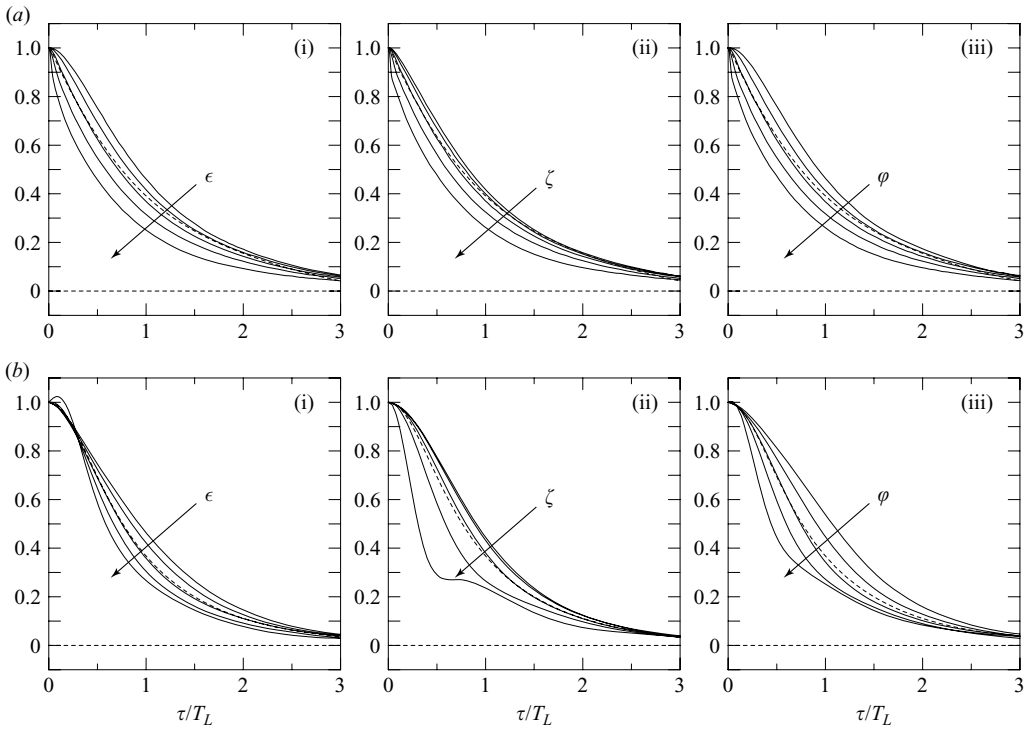
FIGURE 3. Lagrangian velocity autocorrelations conditioned on different values of dissipation, enstrophy and pseudo-dissipation, at (*a*) R_λ approximately 650 and (*b*) 40. Arrows indicate increasing values of conditioning variables ($Z = \epsilon$, ζ or φ) corresponding to $(\ln(Z) - \mu_{(\ln(Z))})/\sigma_{\ln(Z)} = \{-2.054, -0.994, 0, 0.994, 2.054\}$. The unconditional autocorrelation (dashed curve) is included for comparison.

(3.1) since the dissipation–enstrophy cross-correlation is (as seen in figure 1) stronger for $\tau > 0$ than $\tau < 0$. The cross-correlation between ζ and φ is also nearly symmetric, which is due to the dominance of the first term in (3.2).

4. Conditional velocity autocorrelations and local coordinate axes

The autocorrelations of Lagrangian velocity conditioned upon dissipation, enstrophy and pseudo-dissipation provide a direct measure of how local relative motion in the flow affects fluid particle motion. Results at the lowest and highest Reynolds numbers from our simulations are presented in figure 3. As in the Eulerian paper by Yeung *et al.* (2006*a*), because of observed approximate log-normality (especially for pseudo-dissipation) we have chosen conditional sampling intervals based on the standardized logarithms of ϵ, ζ and φ. In particular, for each choice of conditioning variable $Z = \epsilon$, ζ or φ, we have plotted data corresponding to $\ln(Z)$ at its mean value (μ_Z), and approximately ± 1 and ± 2 standard deviations ($\sigma_{\ln Z}$) from the mean.

The general trend, especially at the higher Reynolds number (figure 3*a*), is clearly that velocities of fluid particles experiencing large velocity gradients in the flow tend to decorrelate more rapidly. The conditional autocorrelation at intermediate values of ϵ, ζ or φ is closest to the unconditional autocorrelation (dashed curves) while Reynolds-number dependence seems to be the strongest for ζ as the conditioning
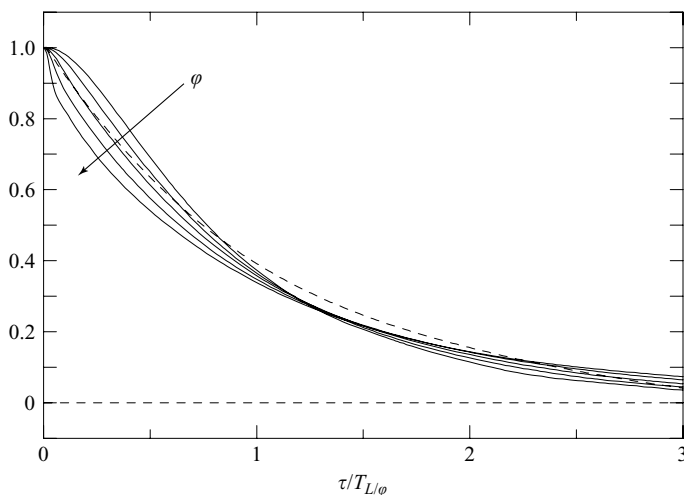
FIGURE 4. Conditional velocity autocorrelation given pseudo-dissipation at $R_\lambda \approx 650$ (same data as figure 3a(iii)), with time lag normalized by conditional integral time scales. The exponential approximation $\exp(-\tau/T_{L|\varphi})$ is shown as a dashed curve.

variable. This is consistent with the Eulerian results of Yeung *et al.* (2006a, figures 7–9 therein) showing that the conditional acceleration variance increases systematically with the conditioning values of dissipation, enstrophy and pseudo-dissipation. The dependence on the conditioning variable is expected to persist in time only as long as the memory of the initial value of ϵ, ζ or φ is sustained. For τ/T_L beyond approximately 3, all of these conditional autocorrelations become nearly zero as the conditioning dependence also trivially vanishes. This result also suggests that although our largest (2048^3) simulation is also the shortest at about 6 T_L, it is still sufficient for the present purposes.

From the perspective of stochastic modelling at high Reynolds number based on the pseudo-dissipation (see discussion in §1), it is useful to know whether the different curves in figure 3(*a*)(iii) can be 'collapsed' into a single form by some alternative scaling on the time-lag axis. Figure 4 provides such a test, in terms of the integral time scale of each conditional autocorrelation. However, it is clear that at small time lags, these curves have a significant difference in shape, which is not removed by the use of a conditional integral time scale.

From a physical perspective, in figure 3(*b*) it is the low-Reynolds-number result, especially for conditioning on enstrophy, that seems to be more intriguing. At low ζ the sensitivity to ζ is very weak, which is consistent with conditional acceleration variances being almost independent of both dissipation and enstrophy in the corresponding data range at low Reynolds numbers (see Yeung *et al.* 2006a, figures 7 and 8 therein). In contrast, at high ζ the conditional dependence is very strong, and the conditional autocorrelation given very large ζ appears to be nearly constant (at about 0.27) for about half a T_L before dropping steadily again with further increase of time lag.

To understand the behaviour noted above it is helpful to study the statistics of velocity components in a local coordinate system evolving with the vorticity vector at each time step, as described in §2. Table 3 shows a comparison of the variances of velocity and acceleration components projected onto axes parallel ($u_\parallel$, $a_\parallel$) and perpendicular ($u_\perp$, $a_\perp$) to the vorticity, with those in fixed Cartesian axes (denoted

N	64	128	256	512	1024	2048
R_λ	43	86	140	235	393	648
$\langle u_\parallel^2 \rangle / \langle u^2 \rangle$	1.13	1.10	1.08	1.05	1.03	1.02
$\langle u_\perp^2 \rangle / \langle u^2 \rangle$	0.94	0.95	0.96	0.97	0.98	0.99
$\langle (\mathrm{d}u_\parallel/\mathrm{d}t)^2 \rangle / \langle a^2 \rangle$	2.34	3.52	4.80	6.95	10.1	14.0
$\langle (\mathrm{d}u_\perp/\mathrm{d}t)^2 \rangle / \langle a^2 \rangle$	2.05	3.41	4.90	7.63	11.6	16.6
$\langle (a_\parallel)^2 \rangle / \langle (\mathrm{d}u_\parallel/\mathrm{d}t)^2 \rangle$	0.208	0.121	0.087	0.060	0.042	0.031
$\langle (u_i \mathrm{d}(\omega_i/\omega)/\mathrm{d}t)^2 \rangle / \langle (\mathrm{d}u_\parallel/\mathrm{d}t)^2 \rangle$	0.703	0.835	0.886	0.926	0.950	0.965
$\langle a_\parallel^2 \rangle / \langle a^2 \rangle$	0.489	0.428	0.427	0.416	0.420	0.434
$\langle a_\perp^2 \rangle / \langle a^2 \rangle$	1.256	1.286	1.286	1.292	1.290	1.285

TABLE 3. Comparison of velocity and acceleration variances in local coordinate axes (based on vorticity) with variances in a standard Cartesian system.

simply as u and a). These results are averaged over three components in fixed axes and two for components in the plane perpendicular to the vorticity vector; orthogonality of axes in both systems requires $3\langle u^2 \rangle = \langle u_\parallel^2 \rangle + 2\langle u_\perp^2 \rangle$ (and similarly for the acceleration). The data indicate that $u_\parallel$ has a larger variance than both u and $u_\perp$, but the difference is small, especially at higher Reynolds numbers where the alignment between velocity and vorticity dominated by large scales and small scales, respectively, is expected to be statistically almost neutral. On the other hand, the ratio of variances between $a_\parallel$ and $a_\perp$ is essentially independent of the Reynolds number. It is possible that the larger variance of $a_\perp$ is due to centripetal accelerations induced in the direction normal to the fluid particle path as a result of vortical motions.

It should be noted that, because of contributions from changes in orientation of the vorticity vector, the time derivatives of $u_\parallel$ and $u_\perp$ are different, and larger, than accelerations in a fixed coordinate frame. In the case of $u_\parallel$, we can write

$$\frac{\mathrm{d}u_\parallel}{\mathrm{d}t} = \frac{\omega_i}{|\boldsymbol{\omega}|}\frac{\mathrm{d}u_i}{\mathrm{d}t} + u_i \frac{\mathrm{d}}{\mathrm{d}t}\left(\frac{\omega_i}{|\boldsymbol{\omega}|}\right), \tag{4.1}$$

where $|\boldsymbol{\omega}|$ is the vorticity magnitude, and the first term is the same as $a_\parallel$, i.e. the acceleration projected in the direction of the vorticity. In table 3, we have included relative contributions of the variances of each term in (4.1) to the variance of the total. It is clear that the second term dominates, especially at higher Reynolds number, accounting for over 96 % of the variances of $\mathrm{d}u_\parallel/\mathrm{d}t$ at $R_\lambda \approx 650$, with the contribution from $a_\parallel$ and a covariance term becoming insignificant. This observation is consistent with the expectation that the vorticity vector undergoes rapid changes in orientation, at time scales shorter than that for the velocity. The Reynolds number trend is also even stronger for $u_\perp$, where rotation of the axes $\boldsymbol{p}$ and $\boldsymbol{q}$ in the orthogonal plane makes further contributions.

The unconditional autocorrelations of u, $u_\parallel$ and $u_\perp$ at different Reynolds numbers are compared in figure 5. Rapid changes in time for $u_\parallel$ and $u_\perp$, as discussed above, are expected to be reflected also in faster decorrelation of these velocity components. Figure 5 shows that $u_\parallel$ remains correlated longer than $u_\perp$, which is consistent with the idea that velocity along the axis of a vortex that maintains its orientation for a finite time changes more slowly than components in the orthogonal plane.

Figure 5 also shows that, as the Reynolds number increases, the contrast among autocorrelations of u, $u_\parallel$ and $u_\perp$ becomes greater since the vorticity vector evolves on short time scales that decrease relative to T_L. A negative 'trough' also begins to
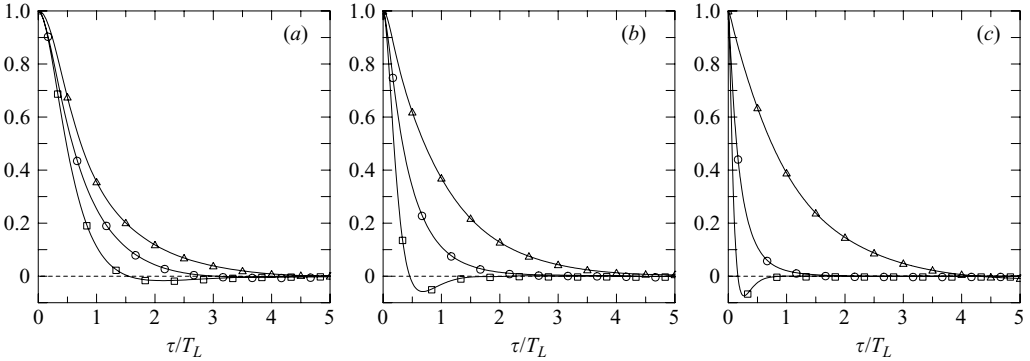
FIGURE 5. Comparison of autocorrelations of velocity component in fixed Cartesian coordinate axes ($\triangle$), and in local axes parallel ($\bigcirc$) and perpendicular ($\square$) to local vorticity vector, at (a) $R_\lambda \approx 40$, (b) 140 and (c) 650.

develop in the autocorrelation of $u_\perp$, with increasing intensity and a zero crossing at a time scale that also decreases relative to T_L. This feature can be described as a damped oscillation, which is consistent with rapid changes in direction of motions in the plane perpendicular to the vorticity vector.

For a closer examination of the behaviour of $u_\parallel$ and $u_\perp$, we show their conditional autocorrelations given the enstrophy in figure 6 at low, intermediate and high Reynolds numbers in our simulations. Because these projected velocity components are defined in a coordinate system moving with the vorticity, the conditional dependence is expected to have a time scale comparable to the integral time scale of enstrophy. Accordingly, we have normalized the time lags in figure 6 by the empirical choice $\sqrt{T_L \tau_\eta}$ suggested by the results of Yeung *et al.* (2006b). It is seen that the conditional autocorrelations indeed fall to zero at several times of $\sqrt{T_L \tau_\eta}$ regardless of the conditioning value. Two remarkable observations can be made: (i) in contrast to other results, the conditional autocorrelation of $u_\parallel$ lasts the longest when the conditioning enstrophy is the largest; and (ii) the conditional autocorrelation of $u_\perp$ shows the 'damped oscillation' type of behaviour seen in figure 5, especially for higher Reynolds number and higher conditioning enstrophy. Both of these features are consistent with the scenario of intense vortices where the axial velocity component changes slowly, but the transverse components evolve rapidly on a time scale that decreases with the local enstrophy used as the conditioning value. The depths of the negative troughs seen in results for $u_\perp$ also reflect greater intensity of local vorticity with increase in Reynolds number or conditioning enstrophy.

Although we observed in figure 4 that the autocorrelation of velocity (in fixed coordinate axes) conditioned on pseudo-dissipation does not scale well with a conditional integral time scale, because of the different physics, a similar concept may be more successful for velocity in local coordinate axes. Indeed, in figure 7 we observe near-perfect universality for $u_\parallel$, especially at high Reynolds number, except for the lowest value of the conditioning enstrophy. However, such a 'collapse' is clearly not possible for the autocorrelations of $u_\perp$ whose shapes (as seen in figure 6b) are very sensitive to the conditioning enstrophy.

In the neighbourhood of a region of high enstrophy, velocity components measured along a set of fixed coordinate axes can be expected to have a behaviour intermediate between the contrasting parallel and perpendicular components presented in figure 6. Specifically, in the $R_\lambda \approx 40$ data, the combination of conditional autocorrelation of $u_\parallel$
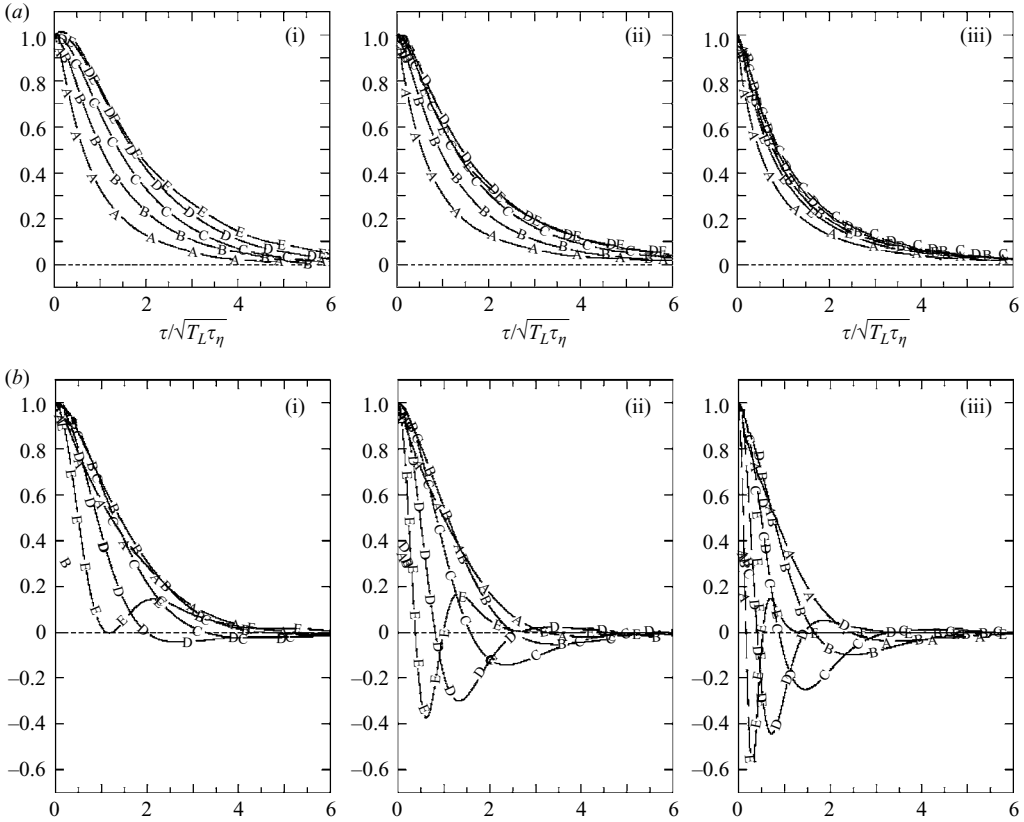
FIGURE 6. Conditional autocorrelations given the enstrophy at (i) $R_\lambda \approx 40$, (ii) 140 and (iii) 650, for (a) $u_\parallel$ and (b) $u_\perp$ in local axes evolving with the vorticity vector. Lines A–E are for increasing values of the conditional enstrophy, at the same levels as those used in figure 3.
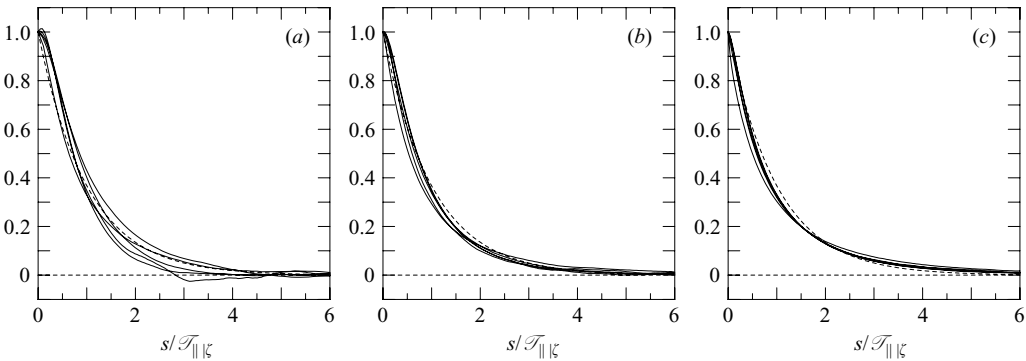

FIGURE 7. Conditional autocorrelations given the enstrophy at (a) $R_\lambda \approx 40$, (b) 140 and (c) 650, for $u_\parallel$ (same data as in figure 6a) with time lag normalized by conditional integral time scale ($\mathscr{T}_{\parallel|\zeta}$). Dashed curve (partly hidden) indicates the exponential approximation $\exp(-\tau/\mathscr{T}_{\parallel|\zeta})$.

decreasing but that of $u_\perp$ increasing with time lag τ in the range between one and two $\sqrt{T_L \tau_\eta}$ is consistent with the observation of conditional autocorrelation levelling out in the range of τ between 0.5 and 1 T_L (figure 3). At higher Reynolds numbers, the

N	64	128	256	512	1024	2048
R_λ	43	86	140	235	393	648
$\langle A_N^2 \rangle / \langle A_P^2 \rangle$	1.71	1.67	1.52	1.42	1.32	1.26

TABLE 4. Variances of parallel and centripetal acceleration components.

damped-oscillation behaviour of the $u_\perp$ conditional autocorrelation is still present, but it occurs at time lags that are very short compared to T_L, i.e. during the range of τ where autocorrelations drop the fastest. As a result, only a small and barely perceptible kink appears in the curve for highest conditioning enstrophy at $R_\lambda \approx 650$ in figure 3.

In the discussions above, the range of time lags where the damped-oscillation effects are significant can be taken to be a measure of the typical time interval that a fluid particle may spend in regions of high vorticity. In other words, the 'blip' in the velocity autocorrelation given high enstrophy (seen in part of figure 3) can be interpreted as a signature of vortex-trapping effects studied by other authors (Biferale *et al.* 2005). However, at higher Reynolds numbers, vorticity time scales become very short and tend to prevent the orientation of a vortex from being maintained for a substantial period of time. Our results are consistent with other sources of DNS data (Biferale & Toschi 2006; Toschi *et al.* 2005) which also showed that vortex trapping may affect Lagrangian statistics on a time scale of a few Kolmogorov time scales.

Additional information on vortex-trapping may also be obtained by considering the centripetal acceleration perpendicular to the velocity vector. We define $A_P = (\boldsymbol{u} \cdot \boldsymbol{a})/|\boldsymbol{u}|$ (which represents changes in velocity magnitude) and a pair of orthogonal components $(A_N^{(1)}, A_N^{(2)})$ in the plane perpendicular to $\boldsymbol{u}$ (which represent changes in direction). Strictly circular motion as in the orthogonal plane of a well-defined line vortex would be reflected in a purely centripetal acceleration, with $A_P = 0$ and the vectors $\boldsymbol{u}$ and $\boldsymbol{a}$ being orthogonal to each other. For stationary isotropic turbulence all of A_P, $A_N^{(1)}$ and $A_N^{(2)}$ have zero mean, whereas their variances are expected to satisfy $\langle A_P^2 \rangle + 2\langle A_N^2 \rangle = \langle \boldsymbol{a} \cdot \boldsymbol{a} \rangle$, where $\langle A_N^2 \rangle$ denotes the variances of both $A_N^{(1)}$ and $A_N^{(2)}$. In our simulations, we find that (table 4) while the importance of centripetal acceleration is indicated by the ratio of variances $\langle A_N^2 \rangle / \langle A_P^2 \rangle$ being larger than unity, this ratio steadily decreases with Reynolds number. The decrease of this ratio is consistent with a shorter duration of vortex trapping effects because this means there are fewer samples of large A_N and small A_P over a finite period of time.

We also show, in figure 8, the PDF of the cosine of the angle (θ) between the vectors $\boldsymbol{u}$ and $\boldsymbol{a}$. A positive value of $\cos\theta$ indicates acute alignment of the vectors $\boldsymbol{u}$ and $\boldsymbol{a}$ and tends to make $|\boldsymbol{u}|$ increase, whereas a negative $\cos\theta$ indicates obtuse alignment which makes $|\boldsymbol{u}|$ decrease. Since the observed $|\boldsymbol{u}|$ is bounded in DNS, negative values of $\cos\theta$ are more likely, which is reflected by a slight deviation from symmetry of the PDF in figure 8. Although this PDF has a peak at $\cos\theta = 0$, it tends to be more spread out at high Reynolds number. However, the difference between data at the two highest Reynolds numbers in this figure is small, which suggests the possibility that the statistics of vectorial alignment between $\boldsymbol{u}$ and $\boldsymbol{a}$ could approach an asymptotic state in the high-Reynolds-number limit.

5. Acceleration, dissipation, enstrophy and pseudo-dissipation

Information on Lagrangian conditional statistics of the acceleration is crucial for our current efforts in stochastic modelling (Lamorgese *et al.* 2007). To illustrate the
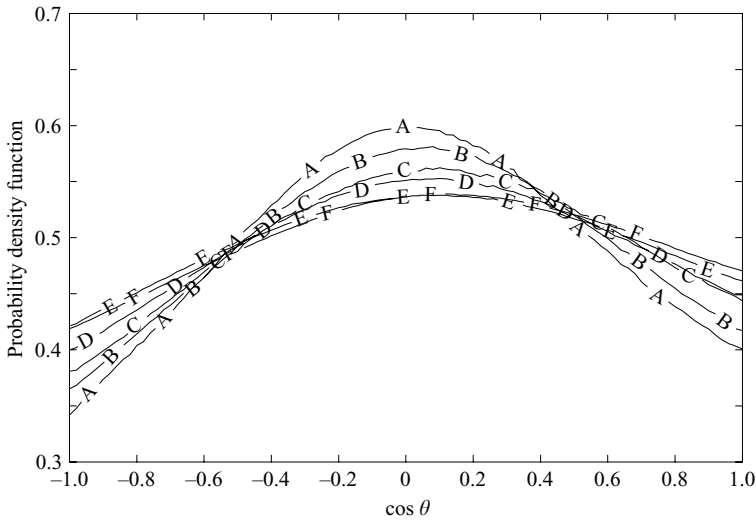
FIGURE 8. PDF of cosine of alignment angle between velocity and acceleration vectors. Lines A–F represent data in ascending order of six different Reynolds numbers from table 1.

connection between acceleration and the conditioning variables ϵ, ζ and φ we show in figure 9 cross-correlation functions between acceleration magnitude (at time t) and dissipation, enstrophy or pseudo-dissipation (at time $t + \tau$), at low, intermediate and high Reynolds numbers. Because large local velocity gradients tend to cause large acceleration, these cross-correlations are positive, and substantial, with the correlation coefficient (at $\tau = 0$) increasing with Reynolds number, as expected. These cross-correlations become narrower with respect to T_L but wider with respect to τ_η, which indicate again the physical process involved has a time scale intermediate between T_L and τ_η. The cross-correlation of acceleration magnitude with pseudo-dissipation is a weighted combination of those with dissipation or enstrophy (Yeung & Pope 1989), and (since enstrophy has a larger variance) is generally closer to the latter. It can be seen that these curves are all asymmetric, but less so at higher Reynolds number. A positive τ may be interpreted as describing the acceleration time history of fluid particles entering a zone of high strain rate (i.e. high ϵ) or high vorticity (i.e. high ζ). At low Reynolds numbers, the observation of $\rho_{|a|\zeta}(\tau)$ being greater than $\rho_{|a|\epsilon}(\tau)$ suggests that fluid particles are drawn into zones of high vorticity more strongly than into zones of high strain rate. The resulting large acceleration is also sustained longer. On the other hand, except for a slight secondary peak in $\rho_{|a|\epsilon}(\tau)$ at low Reynolds number (figures 3a(i) and 3b(i)), for negative τ the three pairs of cross-correlation functions shown are similar. The weaker correlation seen for negative τ suggests that the exit of fluid particles from regions of intense velocity gradients is relatively gradual and not accompanied by large acceleration for a sustained period of time.

The Reynolds-number dependence of the unconditional acceleration autocorrelation (averaged over three coordinate components) is shown in figure 10, with time lag in Kolmogorov variables. In stationary turbulence, the acceleration has a zero integral time scale, which implies mutual cancellation between positive values at small τ and negative values over a more extended range. The property of a zero-crossing time scale being about 2.2 τ_η time scales inferred from lower-Reynolds-number data (Yeung & Pope 1989) remains almost universal, although an increase in the Reynolds number does lead to a more rapid drop within the first two Kolmogorov time scales.
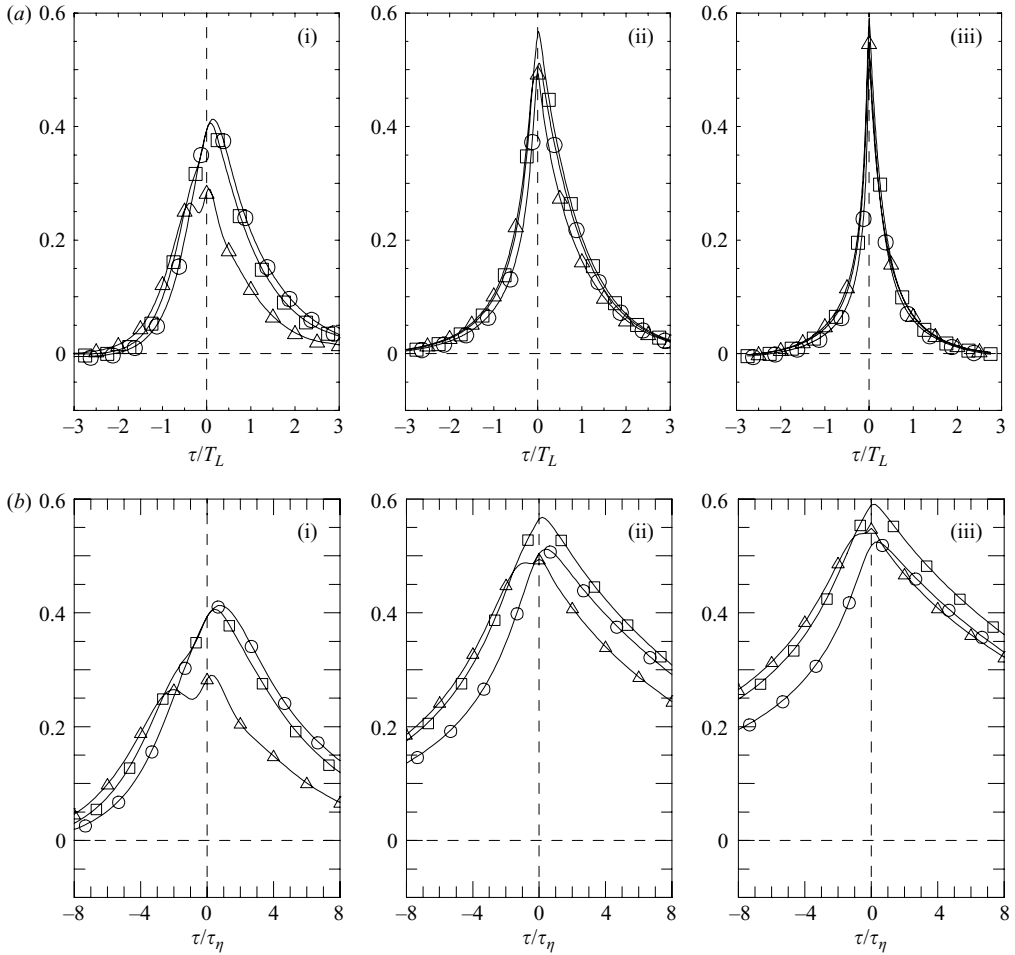
FIGURE 9. Cross-correlation functions $\rho_{|\mathbf{a}|Z}(\tau)$ for Z being dissipation (triangles), enstrophy (circles) and pseudo-dissipation (squares), at (i) $R_\lambda \approx 40$, (ii) 140 and (iii) 650. Normalizing time scales are (*a*) T_L and (*b*) τ_η.

Qualitatively similar results were reported in experiments by Voth *et al.* (1998) in a different flow geometry although a later study (Voth *et al.* 2002) suggested a different picture.

Conditional autocorrelations of the acceleration are shown in figure 11, at the lowest and highest Reynolds numbers simulated, with time lag also in Kolmogorov variables. This autocorrelation function is not subject to the stationarity constraint of zero area under the curve that applies to the unconditional quantity. The general trend is clearly that the acceleration becomes decorrelated earlier with increasing values of the conditioning variables ϵ, ζ and φ, which all represent more intense local velocity gradients in the flow. At high Reynolds numbers, the conditioning dependences on ϵ and φ are stronger than that on ζ, which is consistent with results for the Eulerian conditional acceleration variance (see Yeung *et al.* 2006*a*, figure 10 therein). For the enstrophy at low Reynolds number, there is a non-trivial conditional dependence on ζ only for ζ at relatively large values (curves D and E, in figure 11*b*(ii)). It can also be seen that the unconditional acceleration autocorrelation (dashed curves) is
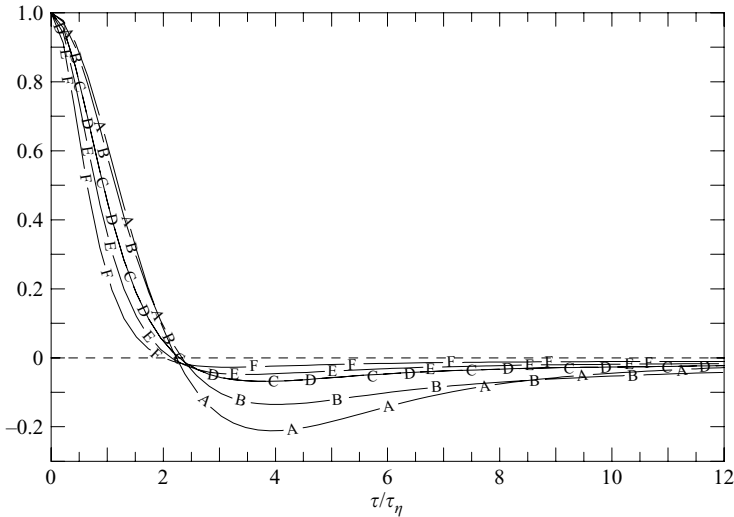
FIGURE 10. Unconditional Lagrangian autocorrelations of (a vector component of) the acceleration at six different Reynolds numbers: $R_\lambda \approx 40$, 90, 140, 240, 390, 650 (lines A–F) corresponding to table 1.

closest to the conditional autocorrelation corresponding to moderately large ϵ, ζ or φ (line D), in contrast to velocity data in figure 3 which showed the best agreement for intermediate values of these conditioning variables. In other words, events of large ϵ, ζ or φ dominate the unconditional acceleration autocorrelation, which can be expected from the strong increase of conditional acceleration variance under such conditions (Yeung *et al.* 2006*a*).

Because figure 11 indicates accelerations of fluid particles in zones of different dissipation or enstrophy evolves on different time scales, it is natural to ask if a local Kolmogorov time scale might be more appropriate for the normalizations. In particular, instead of using $\tau_\eta = \sqrt{\nu/\langle\epsilon\rangle}$, we can ask if a partial 'collapse' of curves can be obtained by using $\hat{\tau}_\eta = \sqrt{\nu/\hat{Z}}$ where $\hat{Z}$ is the conditioning value of Z being ϵ, ζ or φ specific for each curve. However, additional plots (not shown) indicate that this alternative normalization leads to an 'over-correction': i.e. curves plotted versus $\tau/\hat{\tau}_\eta$ follow a trend in Z opposite to that seen in figure 11.

6. Velocity–acceleration joint statistics

In this section, we further characterize the behaviour of velocity and acceleration as a joint stochastic process which is a key component of a new Lagrangian stochastic model described in Lamorgese *et al.* (2007). The simplest joint statistic to consider is the (unconditional) velocity–acceleration cross-correlation function, $\rho_{ua}(\tau) \equiv \langle u(t)a(t+\tau)\rangle/(\sigma_u\sigma_a)$ where σ_u and σ_a are root mean square (r.m.s) velocity and acceleration fluctuations, and averaging over coordinate components is implicit in isotropic turbulence. In stationary turbulence this is an odd function passing through the origin, and (Pope 2000) related to the Lagrangian velocity autocorrelation $\rho_L(\tau)$, as

$$\rho_{ua}(\tau) = \frac{\sigma_u}{\sigma_a}\frac{\mathrm{d}\rho_L(\tau)}{\mathrm{d}\tau}. \tag{6.1}$$
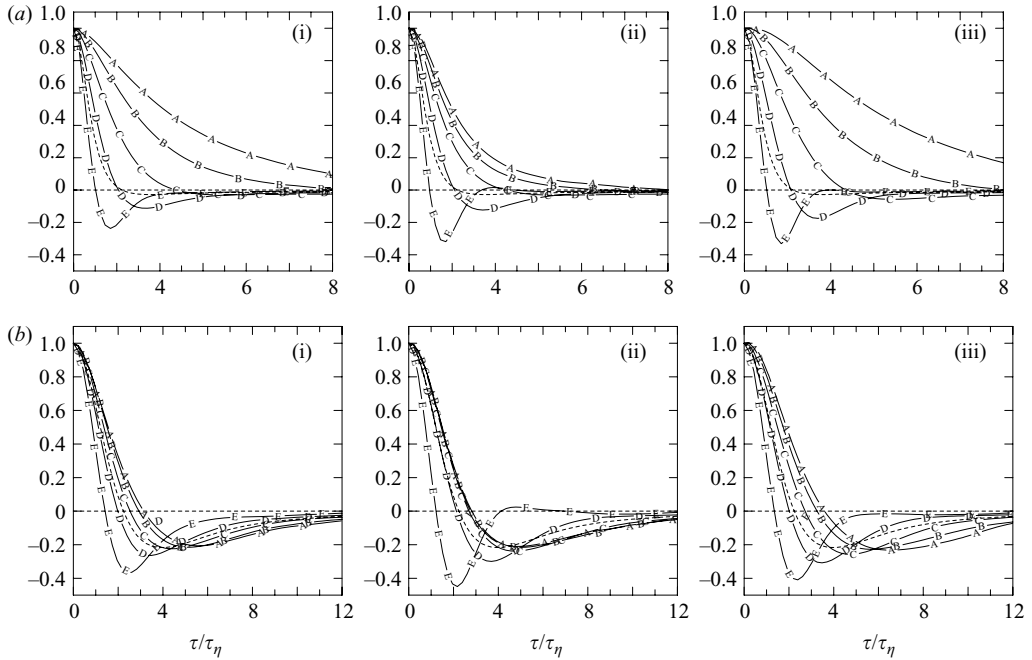
FIGURE 11. Lagrangian acceleration autocorrelations conditioned on different values of dissipation, enstrophy and pseudo-dissipation (same as used in figure 3), from (a) 2048^3 simulation at $R_\lambda \approx 650$ and (b) 64^3 simulation at $R_\lambda \approx 40$. Time lag is normalized by Kolmogorov time scale (τ_η). Unconditional autocorrelations (dashed curve) are included for comparison.

At small τ ($\sim O(\tau_\eta)$), substitution of the parabolic form $\rho_L(\tau) \approx 1 - (\sigma_a \tau/\sigma_u)^2/2$ gives

$$\rho_{ua}(\tau) \approx -\frac{\sigma_a}{\sigma_u}\tau, \qquad (6.2)$$

i.e. a linear regime with negative slope. At large, τ ($O(T_L)$ or larger), the exponential approximation $\rho_L(\tau) \approx \exp(-|\tau|/T_L)$ gives

$$\rho_{ua}(\tau) \approx -\,\mathrm{sgn}(\tau)\frac{\sigma_u}{\sigma_a T_L}\exp(-|\tau|/T_L), \qquad (6.3)$$

which increases with positive τ, but decreases with negative τ. In these expressions, the factor σ_u/σ_a defines a time scale whose Reynolds-number dependence can be be estimated using standard scaling results such as $\langle\epsilon\rangle \approx 15\nu\sigma_u^2/\lambda^2$ (where λ is the Taylor sale), and $\langle\epsilon\rangle \sim 0.4\,\sigma_u^3/L_1$ (Sreenivasan 1998). With $T_L \sim 0.8\,L_1/\sigma_u$ in our DNS (Yeung 2001) we obtain

$$\frac{\sigma_u}{\sigma_a T_L} \approx 6.15\,(a_0 R_\lambda)^{-1/2}, \qquad (6.4)$$

with a_0 being the Kolmogorov-scaled acceleration variance (which increases at least weakly with Reynolds number (Sawford *et al.* 2003; Yeung *et al.* 2006a)). At the same time, we have

$$\frac{\sigma_u}{\sigma_a \tau_\eta} = \frac{(R_\lambda/a_0)^{1/2}}{(15)^{1/4}}, \qquad (6.5)$$

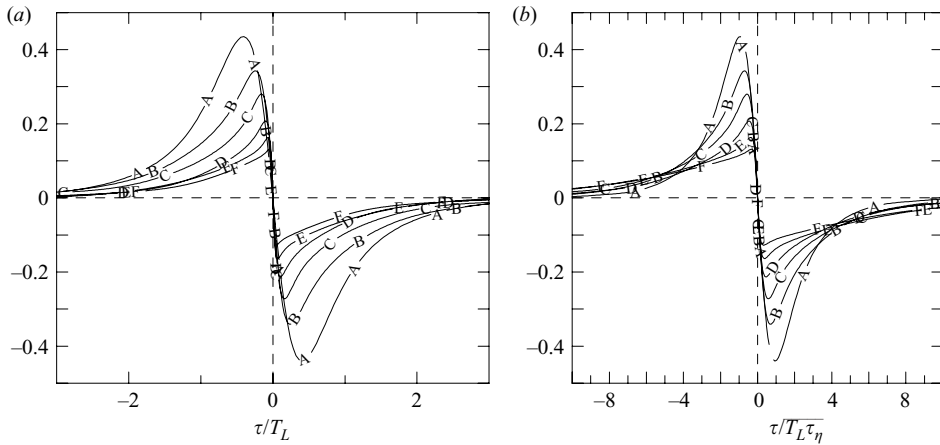thus showing that σ_u/σ_a gives an intermediate time scale between T_L and τ_η.

FIGURE 12. Unconditional Lagrangian velocity–acceleration autocorrelations at different Reynolds numbers (lines A–F, for $R_\lambda \approx 40, 90, 140, 240, 390, 650$), with time lag under two different normalizations.

Figure 12 shows results for $\rho_{ua}(\tau)$ at different Reynolds numbers. It can be seen that $\rho_{ua}(\tau)$ behaves (as expected) as an odd function passing through the origin, with a short linear segment in accordance with (6.2), ultimately followed by decay in a form consistent with (6.3). When plotted versus τ/T_L, an increase of Reynolds number leads to a steeper but shorter linear segment; this can be explained by the slope of the curve being the inverse of (6.4) and noting that τ_η decreases versus T_L so that the exponential decay (6.3) becomes dominant at smaller τ/T_L. Incidentally, since the time-scale ratio T_L/τ_η varies linearly with R_λ, the $R_\lambda^{1/2}$ scaling in (6.4) suggests that a universal collapse of the linear segment is possible if τ is normalized by $\sqrt{T_L \tau_\eta}$ instead. This is verified in figure 12(b).

Conditional cross-correlations are shown in figure 13, between $u^+(t)$ and $a^+(t+\tau)$ (upper half) and between $a^+(t)$ and $u^+(t+\tau)$ (lower half), and for the highest and lowest Reynolds numbers in our simulations. Unlike their unconditional counterparts, conditional cross-correlations are not required to be odd functions, and (in the notation suggested by (2.4)) functions $\rho_{ua}(\tau|Z)$ and $\rho_{au}(\tau|Z)$ are not necessarily equal to the negative of each other. However, it is clear that deviations from antisymmetry (which can be quantified by decomposing these cross-correlations into even and odd parts) are weaker at higher Reynolds number. In other words, such deviations can also be interpreted as low-Reynolds-number effects. Despite the close connection between acceleration and the Kolmogorov time scale, non-zero values of these conditional cross-correlations appear to extend up to time lag of three Lagrangian velocity integral time scales.

Comparison of figure 13 with figure 12 shows that at low values of conditioning ϵ, ζ or φ, the correlation between particle velocity and acceleration tends to persist longer and may reach larger peak values (in magnitude) than in the unconditional cross-correlation. Conversely, it is also clear that velocity and acceleration at different times become uncorrelated faster when under the influence of large ϵ, ζ or φ. This can in part be understood via the effect of a large acceleration which implies rapid changes of the velocity. The greatest effect on the shapes of the curves in figure 13 is that of conditioning enstrophy at low Reynolds number. Similarly to figure 11, the conditional dependence involved is largely restricted to large enstrophy (lines D and E). It may
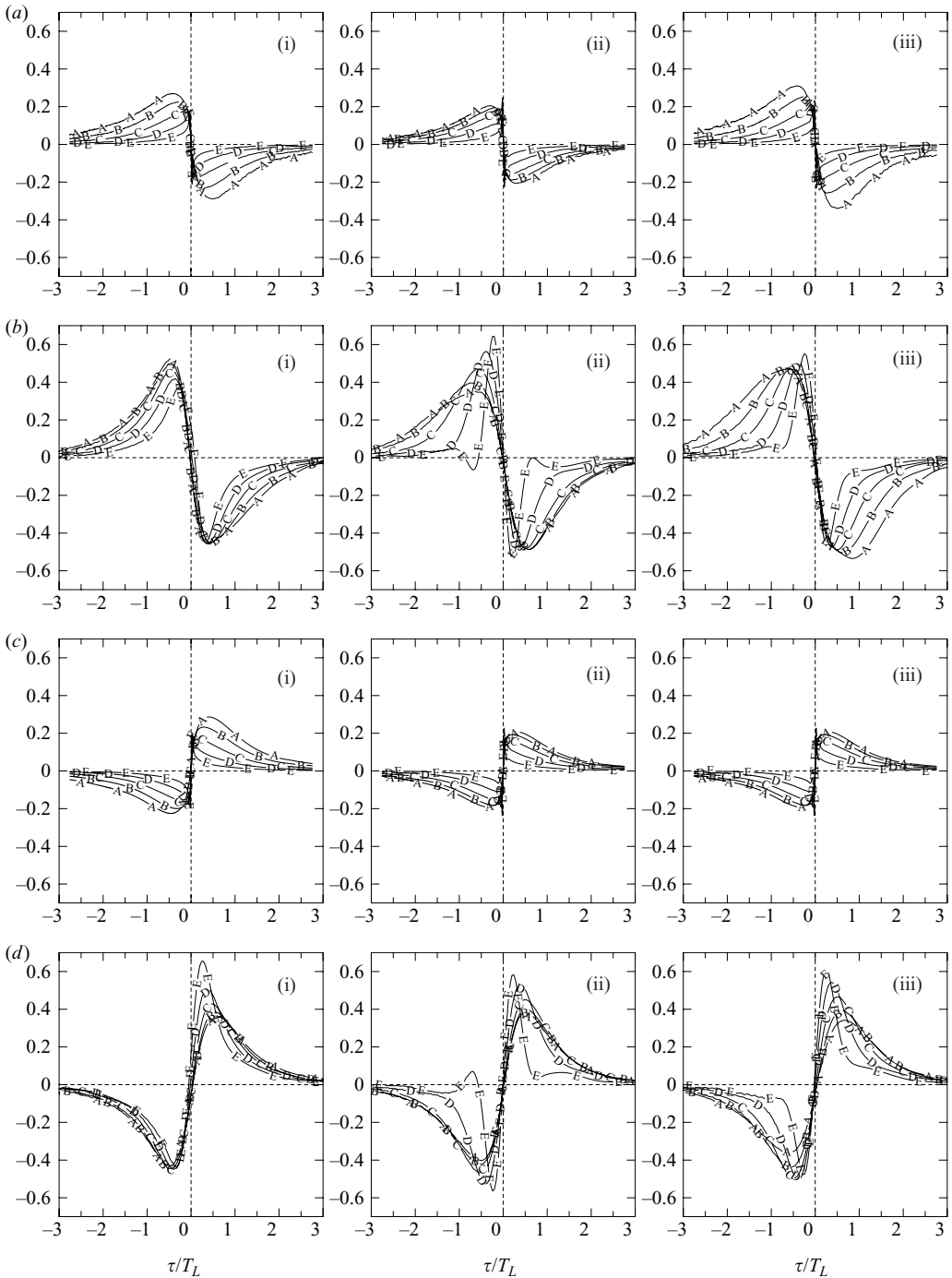
FIGURE 13. Lagrangian cross-correlations between velocity and acceleration conditioned on (i) $Z = \epsilon$, (ii) ζ or (iii) φ. (a) $\rho_{ua}(\tau|Z)$ at $R_\lambda \approx 650$; (b) $\rho_{ua}(\tau|Z)$ at $R_\lambda \approx 40$; (c) $\rho_{au}(\tau|Z)$ at $R_\lambda \approx 650$; (d) $\rho_{au}(\tau|Z)$ at $R_\lambda \approx 40$. The conditioning values for Z in each case are the same as those used in figure 3.

be recognized the conditional cross-correlations shown here are at a level of detail beyond what most current stochastic models (to our knowledge) can predict. Nevertheless, the data presented will be potentially useful for future developments in modelling.

7. Conclusions and discussion

In this paper, we have used direct numerical simulation (DNS) data in forced, stationary isotropic turbulence, at Taylor-scale Reynolds numbers in the range 40–650 and grid resolution 64^3 to 2048^3, to study the effects of spatial intermittency on Lagrangian fluid particle motion including the properties of velocity and acceleration. A primary emphasis is on the behaviour of Lagrangian statistics conditioned on fluctuations of dissipation (ϵ), enstrophy (ζ) and pseudo-dissipation (φ), as extensions of studies of Eulerian conditional statistics of the acceleration (Yeung *et al.* 2006*a*) and the Reynolds-number dependence of basic Lagrangian quantities (Yeung *et al.* 2006*b*). Besides advancing physical understanding, this work also provides data required to test new developments in stochastic modelling incorporating effects of intermittency (Reynolds *et al.* 2005; Lamorgese *et al.* 2007). The Lagrangian conditional statistics presented here are new and involve a degree of detail currently possible only in DNS.

The Lagrangian cross-correlation (in time) between dissipation and enstrophy has an asymmetric form which suggests there is a preferential tendency for fluid particles to experience high dissipation followed by high enstrophy instead of the converse, although this effect becomes weaker at high Reynolds numbers. Conditional auto-correlations of velocity given ϵ, ζ or φ, show clearly that (as expected) the velocities of fluid particles moving in regions of large velocity gradients tend to decorrelate rapidly, in accordance with a large conditional acceleration variance (Yeung *et al.* 2006*a*). However, at low Reynolds number, the conditional autocorrelation given high enstrophy has some distinctive features (figure 3*b*(ii)) which we have examined closely by considering velocity components $u_\parallel$ and $u_\perp$ in a system of local coordinate axes parallel and perpendicular to the vorticity vector. Both $u_\parallel$ and $u_\perp$ evolve and decorrelate rapidly as a result of rapid changes in the vorticity vector orientation, with the autocorrelation of the latter taking on (especially at high Reynolds number) a negative trough typical of systems with damped oscillations. Results for conditional and unconditional autocorrelations of $u_\parallel$ and $u_\perp$ suggest that the 'blip' in figure 3 is a signature of vortex-trapping effects which other authors (e.g. Biferale *et al.* 2005) have reported to have a time scale of several Kolmogorov time scales. Additional information is also presented in terms of centripetal acceleration projected along the direction of the velocity vector. At higher Reynolds number, since the vorticity then evolves on shorter time scales, a strong vortex in the flow is probably not well sustained in time.

Results on the cross-correlations between acceleration magnitude ($|\boldsymbol{a}|$) and the variables ϵ, ζ and φ suggest that fluid particles are drawn into zones of high vorticity with a larger acceleration compared with zones of high strain rate, although the contrast becomes weaker at high Reynolds number. At high Reynolds numbers, conditional acceleration autocorrelations show a very strong dependence on the conditioning variables, especially for dissipation and pseudo-dissipation (figure 11*a*). Although the conditional acceleration evolves on a time scale that decreases with the intensity of local velocity gradients, normalization by a local Kolmogorov time scale based on the conditioning variables does not produce a close 'collapse' of the data.

For a further characterization of the conditional joint distribution of velocity and acceleration, we have also presented cross-correlations between the velocity and acceleration. The unconditional cross-correlation is shown to be characterized by a

short linear segment followed by an exponential decay related to the shape of the velocity autocorrelation. The conditional cross-correlation departs from antisymmetry primarily at low Reynolds number, where high conditioning enstrophy again leads to qualitatively different results.

In summary, we have presented here new results from numerical simulations up to 2048^3 grid resolution on the conditional statistics of Lagrangian fluid-particle motion, where several features associated with low Reynolds number have been identified. While contrasts between conditioning on dissipation and on enstrophy give useful information on the physics of intermittency effects, pseudo-dissipation is (as suggested by Yeung *et al.* 2006*a*) the best conditioning variable for use in modelling. The body of data presented here, as well as the underlying simulation database, is expected to be useful in the development of Lagrangian stochastic models, such as the conditionally cubic Gaussian model for velocity, acceleration and pseudo-dissipation, developed by Lamorgese *et al.* (2007).

REFERENCES

BEC, J., BIFERALE, L., CENCINI, M., LANOTTE, A. & TOSCHI, F. 2006 Effect of vortex filaments on the velocity of tracers and heavy particles in turbulence. *Phys. Fluids* **18**, 081702.

BERG, J., LUTHI, B., MANN, J. & OTT, S. 2006 Backwards and forwards relative dispersion in turbulent flow: an experimental investigation. *Phys. Rev.* E **74**, 016304.

BIFERALE, L. & TOSCHI, F. 2006 Joint statistics of acceleration and vorticity in fully developed turbulence. *J. Turbulence* **6** (10), 1–8.

BIFERALE, L., BOFFETTA, G., CELANI, A., DEVENISH, B. J., LANOTTE, A. & TOSCHI, F. 2004 Multifractal statistics of Lagrangian velocity and acceleration in turbulence. *Phys. Rev. Lett.* **93**, 064502.

BIFERALE, L., BOFFETTA, G., CELANI, A., LANOTTE, A. & TOSCHI, F. 2005 Particle trapping in three-dimensional fully developed turbulence. *Phys. Fluids* **17**, 021701.

CHEN, S., SREENIVASAN, K. R. & NELKIN, M. 1997 Inertial range scalings of dissipation and enstrophy in isotropic turbulence. *Phys. Rev. Lett.* **79**, 1253–1256.

CHEVILLARD, L., ROUX, S. G., LEVEQUE, E., MORDANT, N., PINTON, J. F. & ARNEO, A. 2003 Lagrangian velocity statistics in turbulent flows: effects of dissipation. *Phys. Rev. Lett.* **91**, 214502.

CRAWFORD, A. M., MORDANT, N. & BODENSCHATZ, E. 2005 Joint statistics of the Lagrangian acceleration and velocity in fully developed turbulence. *Phys. Rev. Lett.* **94**, 024501.

ESWARAN, V. & POPE, S. B. 1988 An examination of forcing in direct numerical simulations of turbulence. *Computers Fluids* **16**, 257–278.

GUALA, M., LIBERZON, A., KINZELBACH, W. & TSINOBER, A. 2006 Stretching and tilting of material lines in turbulence: the effect of strain and vorticity. *Phys. Rev.* E **73**, 036303.

KRONENBURG, A. & BILGER, R. W. 1997 Modelling of differential diffusion effects in nonpremixed nonreacting turbulent flow. *Phys. Fluids* **9**, 1435–1447.

LAPORTA A., VOTH, G. A., CRAWFORD, A. M., ALEXANDER, J. & BODENSCHATZ, E. 2001 Fluid particle accelerations in fully developed turbulence. *Nature* **409**, 1017.

LAMORGESE, A. G., POPE, S. B., YEUNG, P. K. & SAWFORD, B. L. 2007 A conditionally cubic-Gaussian stochastic Lagrangian model for acceleration in isotropic turbulence. *J. Fluid Mech.* **582**, 423–448.

LUTHI, B., TSINOBER, A. & KINZELBACH, W. 2005 Lagrangian measurement of vorticity dynamics in turbulent flow. *J. Fluid Mech.* **528**, 87–118.

MONIN, A. S. & YAGLOM, A. M. 1975 *Statistical Fluid Mechanics*, vol. 2. MIT Press, Cambridge, MA.

MORDANT, N., METZ, P., MICHEL, O. & PINTON, J.-F. 2001 Measurement of Lagrangian velocity in fully developed turbulence. *Phys. Rev. Lett.* **87**, 214501.

MORDANT, N., CRAWFORD, A. M. & BODENSCHATZ, E. 2004 Experimental Lagrangian acceleration probability density function measurement. *Physica* D **193**, 245–251.

NELKIN, M. 1999 Energy and dissipation must have the same scaling exponent in the high Reynolds number limit of fluid turbulence. *Phys. Fluids* **11**, 2202–2204.

OUELLETTE, N. T., XU, H. T. & BODENSCHATZ, E. 2006 A quantitative study of three-dimensional Lagrangian particle tracking algorithms. *Exps. Fluids* **40**, 301–313.

POPE, S. B. 1985 PDF methods for turbulent reactive flows. *Prog. Energy Combust. Sci.* **11**, 119–192.

POPE, S. B. 2000 *Turbulent Flows.* Cambridge University Press.

POPE, S. B. 2002 A stochastic Lagrangian model for acceleration in turbulent flows. *Phys. Fluids* **14**, 2360–2375.

POPE, S. B. & CHEN, Y. L. 1990 The velocity-dissipation probability density function model for turbulent flows. *Phys. Fluids* A **2**, 1437–1449.

REYNOLDS, A. M. 2003*a* On the application of non-extensive statistics to Lagrangian turbulence. *Phys. Fluids* **15**, L1.

REYNOLDS, A. M. 2003*b* Superstatistical mechanics of tracer particle motions in turbulence. *Phys. Rev. Lett.* **91**, 084503.

REYNOLDS, A. M., MORDANT, N., CRAWFORD, A. M. & BODENSCHATZ, E. 2005 On the distribution of Lagrangian accelerations in turbulent flows. *New J. Phys.* **7**, art. 58.

ROGALLO, R. S. 1981 Numerical experiments in homogeneous turbulence. *NASA T.M* 81315.

SAWFORD, B. L. 1991 Reynolds number effects in Lagrangian stochastic models of turbulent dispersion. *Phys. Fluids* A **3**, 1577–1586.

SAWFORD, B. L. 2001 Turbulent relative dispersion. *Annu. Rev. Fluid Mech.* **33**, 289–317.

SAWFORD, B. L., YEUNG, P. K., BORGAS, M. S., VEDULA, P., CRAWFORD, A. M., LAPORTA, A. & BODENSCHATZ, E. 2003 Acceleration variance and conditional variance statistics in turbulence. *Phys. Fluids* **15**, 3478–3489.

SREENIVASAN, K. R. 1998 An update on the dissipation range in homogeneous turbulence. *Phys. Fluids* **10**, 528–529.

SREENIVASAN, K. R. & ANTONIA, R. A. 1997 The phenomenology of small-scale turbulence. *Annu. Rev. Fluid Mech.* **29**, 435–472.

TAYLOR, G. I. 1921 Diffusion by continuous movements. *Proc. Lond. Math. Soc. Ser. 2* **20**, 196–211.

TOSCHI, F., BIFERALE, L., BOFFETTA, G., CELANI, A., DEVENISH, B. J. & LANOTTE, A. 2005. Acceleration and vortex filaments in turbulence. *J. Turbulence* **6** (15), 1–10.

VEDULA, P., YEUNG, P. K. & FOX, R. O. 2001 Dynamics of scalar dissipation in isotropic turbulence: a numerical and modelling study. *J. Fluid Mech.* **433**, 29–60.

VOTH, G. A., SATYANARAYAN, K. & BODENSCHATZ, E. 1998 Lagrangian acceleration measurements at large Reynolds number. *Phys. Fluids* **10**, 2268–2280.

VOTH, G. A., LAPORTA, A., CRAWFORD, A. M., ALEXANDER, J. & BODENSCHATZ, E. 2002 Measurement of particle accelerations in fully developed turbulence. *J. Fluid Mech.* **469**, 121–160.

XU, H. T., OUELLETTE, N., BOURGOIN, M. & BODENSCHATZ, E. 2006 Lagrangian velocity structure functions in high Reynolds number turbulence. *Phys. Rev. Lett.* **96**, 024503.

YAKHOT, V. & SREENIVASAN, K. R. 2005 Anomalous scaling of structure functions and dynamic constraints in turbulence simulations. *J. Stat. Phys.* **121**, 823–841.

YEUNG, P. K. 1997 One- and two-particle Lagrangian acceleration correlations in numerically simulated homogeneous turbulence. *Phys. Fluids* **9**, 2981–2990.

YEUNG, P. K. 2001 Lagrangian characteristics of turbulence and scalar transport in direct numerical simulations. *J. Fluid Mech.* **427**, 241–274.

YEUNG, P. K. 2002 Lagrangian investigations of turbulence. *Annu. Rev. Fluid Mech.* **34**, 115–142.

YEUNG, P. K. & POPE, S. B. 1988 An algorithm for tracking fluid particles in numerical simulations of homogeneous turbulence. *J. Comput. Phys.* **79**, 373–416.

YEUNG, P. K. & POPE, S. B. 1989 Lagrangian statistics from direct numerical simulations of isotropic turbulence. *J. Fluid Mech.* **207**, 531–586.

YEUNG, P. K. & ZHOU, Y. 1997 On the universality of the Kolmogorov constant in numerical simulations of turbulence. *Phys. Rev.* E **56**, 1746–1752.

YEUNG, P. K., DONZIS, D. A. & SREENIVASAN, K. R. 2005 High Reynolds number simulation of turbulent mixing. *Phys. Fluids* **17**, 081703.

YEUNG, P. K., POPE, S. B., LAMORGESE, A. G. & DONZIS, D. A. 2006a Acceleration and dissipation statistics of numerically simulations of isotropic turbulence. *Phys. Fluids* **18**, 065103.

YEUNG, P. K., POPE, S. B. & SAWFORD, B. L. 2006b Reynolds number dependence of Lagrangian statistics in large numerical simulations of isotropic turbulence. *J. Turbulence* **7**(58), 1–12.

ZHOU, T. & ANTONIA, R. A. 2000 Reynolds number dependence of the small-scale structure of grid turbulence. *J. Fluid Mech.* **406**, 81–107.